RESEARCH ARTICLE | OCTOBER 04 2023

Ferroelectric Schottky diodes of CuInP₂S₆ nanosheet •

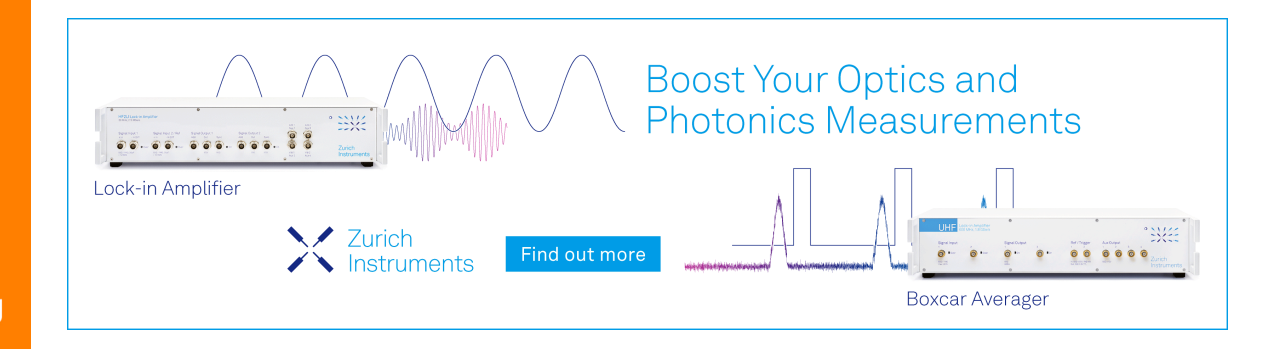
Jinyuan Yao ^⑤ ; Yongtao Liu ^⑥ ; Shaoqing Ding ^⑥ ; Yanglin Zhu ^⑥ ; Zhiqiang Mao ^⑥ ; Sergei V. Kalinin ^⑥ ; Ying Liu ☑ ^⑥



Appl. Phys. Lett. 123, 142903 (2023) https://doi.org/10.1063/5.0160928









Ferroelectric Schottky diodes of CuInP₂S₆ nanosheet (1)

Cite as: Appl. Phys. Lett. **123**, 142903 (2023); doi: 10.1063/5.0160928 Submitted: 6 June 2023 · Accepted: 20 September 2023 · Published Online: 4 October 2023







Jinyuan Yao, Dongtao Liu, Dongt

AFFILIATIONS

- ¹Department of Physics and Materials Research Institute, The Pennsylvania State University, University Park, Pennsylvania 16802, USA
- 2 Center for Nanophase Materials Sciences, Oak Ridge National Laboratory, Oak Ridge, Tennessee 37831, USA
- ³Nanjing Normal University, Nanjing, Jiangsu 210023, China
- 4 Department of Materials Science and Engineering, The University of Tennessee, Knoxville, Tennessee 37996, USA

ABSTRACT

Ferroelectricity in van der Waals (vdW) layered material has attracted a great deal of interest recently. $CuInP_2S_6$ (CIPS), the only vdW layered material whose ferroelectricity in the bulk was demonstrated by direct polarization measurements, was shown to remain ferroelectric down to a thickness of a few nanometers. However, its ferroelectric properties have just started to be explored in the context of potential device applications. We report here the preparation and measurements of metal-ferroelectric semiconductor-metal heterostructures using nanosheets of CIPS obtained by mechanical exfoliation. Four bias voltage and polarization dependent resistive states were observed in the current–voltage characteristics, which we attribute to the formation of ferroelectric Schottky diode, along with switching behavior.

Published under an exclusive license by AIP Publishing. https://doi.org/10.1063/5.0160928

Ferroelectric semiconductors can have interesting properties that are potentially useful for microelectronic applications. For example, when a ferroelectric semiconductor is in a close electrical contact with a metal, ferroelectric polarization can have a strong effect on the Schottky barrier and the depletion near the interface, leading to rectifying behavior and ferroelectric Schottky diodes (FSDs). So far FSDs have been studied using mostly an oxide as the ferroelectric layer, including PbTiO₃ (Ref. 3), BiFeO₃ (Refs. 2 and 4), Pb(Zr_{0.2}Ti_{0.8})O₃ (Ref. 5), and Zn_xCd_{1-x}S (Ref. 6). The polarization was found to control the resistive state of FSD, which may be useful for nonvolatile memory applications. Comparing with the traditional one-transistor-one-capacitor ferroelectric random access memory (1T1C FeRAM) whose read/write process is destructive, FSDs have the potential to achieve improved endurance due to its nondestructive readout process.

Van der Waals (vdW) layered ferroelectric semiconductors that can be exfoliated into nanosheets are attractive for the study of FSD as an atomically sharp interface with a metal can be obtained. CuInP₂S₆ (CIPS) features a layered monoclinic crystalline structure [Figs. 1(a) and 1(b)] with a c-axis lattice constant roughly 1.36 nm. The bulk ferroelectric transition temperature (T_c) was found to be around 315 K, with a remnant polarization of 2.55 μ C/cm² and a coercive field of

77 kV/cm. More recent measurements suggest that the bulk remnant polarization can be as high as $4.5\,\mu\text{C/cm}^2$ with a coercive field as low as $30\,\text{kV/cm}$. Piezoelectric force microscopy (PFM) suggests that piezoelectricity and ferroelectricity persist down to a 4 nm thickness even though its remnant polarization cannot be measured due to leakage current. As-grown crystals of CIPS are typically hole-doped semiconductors 13,14 with a bandgap of $2.8\,\text{eV}$. The suggestion of the bulk remnant polarization cannot be measured as 13,14 with a bandgap of 13,14 with a bandgap of 13 0. The bulk remnant polarization cannot be measured due to leakage current.

Switchable behavior was found previously in metal-CIPS-metal structures. $^{16-20}$ However, the connection between the observed switchable behavior and the switching of the polarization in the ferroelectric layer was not well established. A potential issue is that the existence of vacancies and charge traps at the interfaces may also lead to switching behavior. In the current study, we prepared Au/CIPS/Cr and Au/CIPS/Ni metal-ferroelectric-metal heterostructures and demonstrated resistive switchings with an ON/OFF ratio up to 10^3 , as shown previously in the studies of $BaZrO_3/SrRuO_3$ structures 21 and Sr doped $BiFeO_3$ thin films. 22 The issue of vacancy and Cu ion motion vs polarization switching was explored by examining behaviors of devices of different thickness and electrodes.

Thin and ultrathin crystals of CIPS were obtained from single crystals grown by chemical vapor transport (CVT).²³ To grow single crystals of CIPS, Cu, In, P, and S powder were mixed in a

^{a)}Author to whom correspondence should be addressed: yxl15@psu.edu

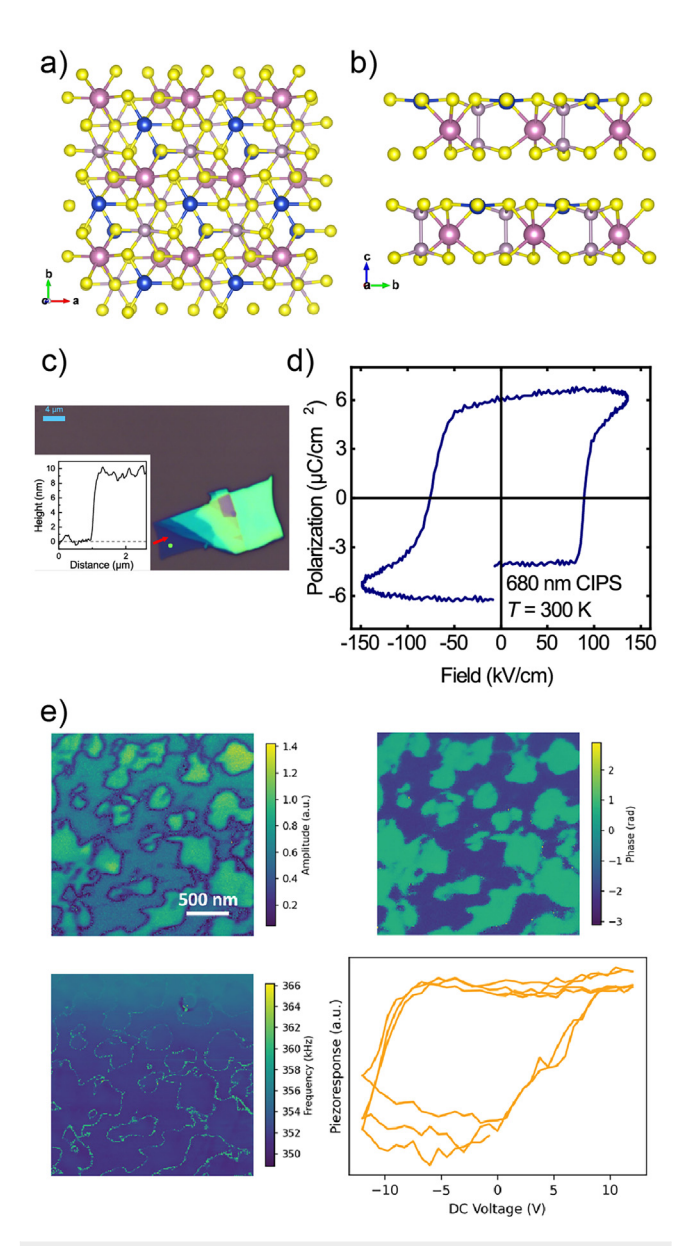


FIG. 1. Structure and material characterization of CIPS. (a) and (b) Top and side views of the crystal structure of CuInP $_2$ S $_6$. (c) Atomic force microscopy (AFM) of an exfoliated nanosheet of CIPS. A line scan is shown in the inset. (d) Hysteresis loop from a 680-nm-thick crystal of CIPS measured at room temperature. (e) Piezoforce force microscopy (PFM) characterization of a thin crystal of CIPS on top of bottom electrode formed by 5 nm thick Ti and 45 nm Au films deposited on a Si substrate with thermally grown SiO $_2$ surface.

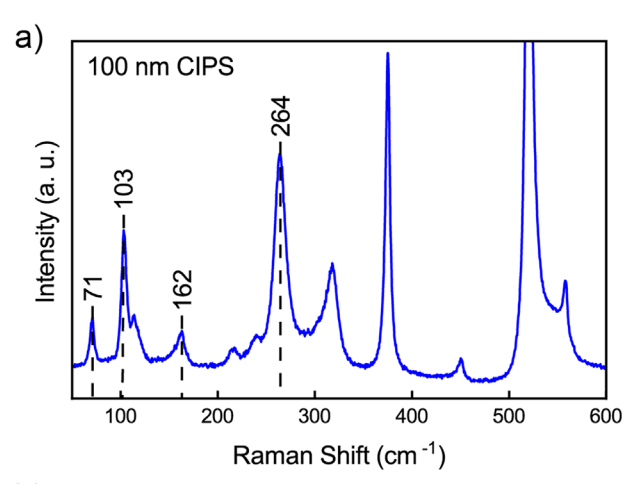
stoichiometric ratio and loaded into a quartz tube (10 mm in diameter and 18 cm length). The transport agent, I₂, was added. The quartz tube was sealed under vacuum and then heated up in a horizontal doublezone furnace with the hot and cold ends set at 750 and 650 °C, respectively. After 14 days, the furnace was shut down, and the quartz tube was naturally cooled down to room temperature. The yellow plate-like single crystals were found at the cold end of the quartz tube. CIPS

crystals were mechanically exfoliated onto polydimethylsiloxane (PDMS) and then transferred onto the bottom electrode prepared by depositing 5 nm thick Ti followed by 45 nm thick Au on a Si/SiO $_2$ substrate. The thickness of cleaved crystal was estimated by its color and faintness under the optical microscope and determined more precisely using atomic force microscopy (AFM) (Bruker Dimension). Top electrodes were made by e-beam deposition of Ni (20 nm thick) and Au (30 nm thick) or Cr (20 nm thick) and Au (30 nm thick) sequentially followed by maskless photolithography. Raman measurements were conducted on Horiba LabRAM HR. DC current–voltage measurements were conducted on probe station Form Factor 11000B with the Keithley 4200-SCS Parameter Analyzer.

In Fig. 1(d), we show a hysteresis loop of a 680-nm-thick CIPS crystal obtained by mechanical exfoliation and polarization vs electric field [P(E)]. For this structure, the bottom and top electrodes (BE and TE) are Au and Pt, respectively. Thinner crystals of CIPS can also be obtained as shown in Fig. 1(c). At such thickness, the polarization is difficult to measure because the leakage currents are usually very large. The remnant polarization P_r and coercive field E_c in the bulk are $2.55\,\mu\text{C/cm}^2$ and $77\,\text{kV/cm}$, respectively. For our thick crystals, the P_r and E_c were found to be $6\,\mu\text{C/cm}^2$ and $89\,\text{kV/cm}$, respectively. The open hysteresis loop seen in Fig. 1(d) indicates that the polarization state did not recover its initial state after the electrical sweep due to incomplete switching of domains or the presence of defects.

We carried out Raman spectroscopy measurements of thin crystals of CIPS as its thickness is reduced. Figure 2(a) shows the Raman spectrum of a 100-nm-thick CIPS flake. Four peaks that are only present in ferroelectric phase (71, 103, 162, and $264 \,\mathrm{cm}^{-1}$)²⁵ were observed. The peak at 71 cm⁻¹ is related to the out-of-plane motion of Cu ions, which is believed to be responsible to the ferroelectricity in CIPS. 15 Other peaks correspond to the out-of-plane motion of P-P dimers and in-plane motion of S atoms. Figure 2(b) shows the Raman spectra from thin and ultrathin crystals of CIPS with different thicknesses ranging from 10 to 110 nm. All four peaks mentioned above are seen with their positions essentially the same as the thickness is reduced, suggesting that the ferroelectricity is robust down to 10 nm. However, significant changes are seen in two peaks found at 317 and 558 cm⁻¹, respectively, which are not changed significantly until the thickness becomes smaller than 33 nm. As the thickness decreases further, the $317 \, \text{cm}^{-1}$ shifts to lower wave number, while the width of this peak increases. The peak at 558 cm⁻¹ does not shift, but the intensity of this peak decreases as the thickness goes down. For 15- and 10-nmthick crystals, this peak essentially vanishes. The implications of these observations are to be understood.

In Fig. 3, the curves of current density (J) vs applied electric field (E_a) (J– E_a) are shown for four heterostructures prepared on 200- and 33-nm-thick crystals of CIPS, with BEs of all four devices Au (with a Ti underlay) and the TEs Cr and Ni (with an Au overlay), respectively. Hysteresis loops were observed in all four devices. For the two devices with Ni as the TE, two deep minima are seen at two different non-zero values of E_a . When the magnitude of E_a increases for both the positive and negative biases, the Ni-200 nm device was found to show an initial increase in J, a drop, and then a rise sharply again at higher E_a values starting around 75 kV/cm, which is roughly the reported coercive fields of bulk CIPS. 16,24 For the Ni-33 nm device, the corresponding values for the sharp rise in J are 450 kV/cm on the positive and -330 kV/cm on the negative side of E_a , also consistent with increased coercive field



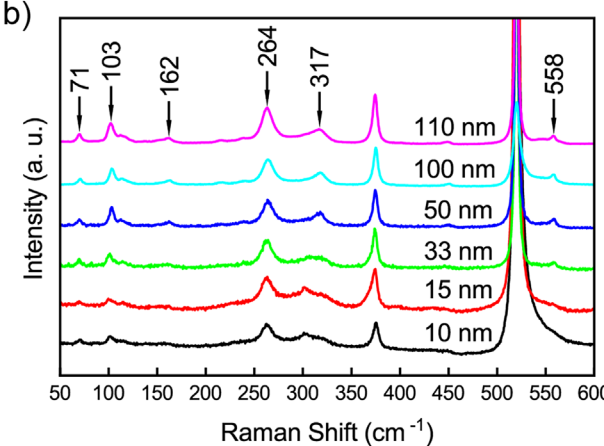


FIG. 2. Raman spectra of thin CIPS crystals. (a) Raman spectrum of a 100-nm-thick CIPS crystal. Four peaks that only occur in the ferroelectric phase are labeled. (b) Thickness dependence of Raman spectra of CIPS. Peaks that change significantly as thickness decreases are labeled.

of thin crystals of CIPS. Therefore, the rapid increase in J appears to be associated with the switching of the ferroelectric polarization. Indeed, the butterfly-shaped hysteresis in the J- E_a curves of these two heterostructures is qualitatively consistent with the ferroelectric switching.

However, complex behavior was also found in devices featuring a Ni TE. For the Ni-200 nm device, the drop of J after reaching two secondary peaks as described above suggests the depletion of mobile charges even as the magnitude of E_a was increasing. Moreover, the ratio of upper branch to lower branch of the hysteresis loop on the negative bias side is much smaller than the ratio on the positive bias side. For the Ni-33 nm device, the hysteresis loop on the negative bias side actually has a different direction than that of the Ni-200 nm device, as seen in Figs. 3(c) and 3(d).

For devices with a Cr TE [Figs. 3(e) and 3(f)], the behavior seems to be simpler than those with Ni as TE. The secondary peaks seen in J– E_a curves of the Ni-200 nm device are absent in both the positive and negative voltage sweeps. Interestingly, the J– E_a curves are seen to stay relatively flat at the low bias voltages, making the negative-to-positive sweeps symmetric without showing rectification. In addition, J values

in the J– E_a curves for the positive to zero sweep are small, and the hysteresis loop in the J– E_a curve becomes counterclockwise for both devices.

Similar J– E_a characteristics were seen previously in BiFeO₃ (Ref. 26), which were attributed to the defects formed during the synthesis. The important question is whether the switching behavior seen in the present work can also be related to defects or ionic motion in CIPS. Indeed, sulfur vacancies are common in CIPS due to its volatility, resulting in the 2p peak shift seen previously in the X-ray photo spectroscopy (XPS) studies. ¹⁴ In addition, it has been widely reported ¹ that mobile Cu ions are present in CIPS, which would, in principle, also affect the conductivity of our devices. However, it is unlikely that the motion of S vacancies and/or Cu ions plays an important role in our devices. First, the voltage was swept at around 1.3 V/s, which is so slow that the hysteresis from Cu ion migration should only appear on one side of the voltage sweeping, 18 opposite from what was seen experimentally. In addition, the motion of the S vacancies and/or Cu ions is unlikely to be affected by the electrodes as they reside mostly in the interior of the CIPS crystals, which is also different from what was seen experimentally. We propose that the formation of a Schottky barrier in a ferroelectric semiconductor and the effect of polarization on the barrier height is responsible to the characteristics of our devices. The relative positions of vacuum levels, Fermi levels, and conduction band minima of metal electrodes and CIPS are shown in Fig. 4(a). The depletion width without bias can be estimated by²

$$W = \sqrt{\frac{2\epsilon\epsilon_0 V_{bi}}{qN_A}},\tag{1}$$

where ϵ , V_{bi} , q, and N_A represent dielectric constant of CIPS, built-in potential, elementary charge, and density of the acceptors. According to a previous report, dielectric constant of CIPS is 40 (Ref. 15). When $V_{bi}=1.5 \, \mathrm{V}$ and $N_A=10^{18} \, \mathrm{cm}^{-3}$, depletion width W is around 80 nm, much larger than 33 nm. Thus, 33 nm CIPS should be fully depleted.

A Schottky barrier is formed with band bending expected only in thick CIPS but not in thin ones as stated earlier. When the polarization is present in CIPS, the negative bound charge tends to suppress the Schottky barrier, while the positive bound charge will increase the Schottky barrier height at the interface [Figs. S4(b) and S4(c)]. The device can be modeled as a diode with the Schottky barrier height controlled by the ferroelectric polarization. In devices prepared on the thin crystal, the CIPS is totally depleted, so the band bending cannot form [Fig. 4(b)]. The heights of the Schottky barriers on the two interfaces and the sample resistance are affected by the polarization. When the polarization points are down (toward Au electrode), the barrier height on Cr-CIPS or Ni-CIPS interface is larger without bias voltage. When negative bias voltage is applied [Figs. 4(c) and 4(e)], barrier height for electron transport is lowered, leading to a low resistance state. Positive bias voltage would then correspond to a high resistance state [Fig. 4(d)]. When polarization points are up, in the Cr-33 nm device, Au-CIPS interface has a larger barrier height. Thus, the device is in low resistance state when positive bias voltage is applied [Fig. 4(f)]. For the Cr-33 nm device, the device behaves as a diode that is forward biased when the applied field is parallel with depolarization field [Figs. 4(c) and 4(f)], leading to the butterfly-shape $J-E_a$ curves in Fig. 3(f). The difference between the hysteresis directions of Cr-33 nm and Ni-33 nm devices may be attributed to the different work functions of Cr and Ni.

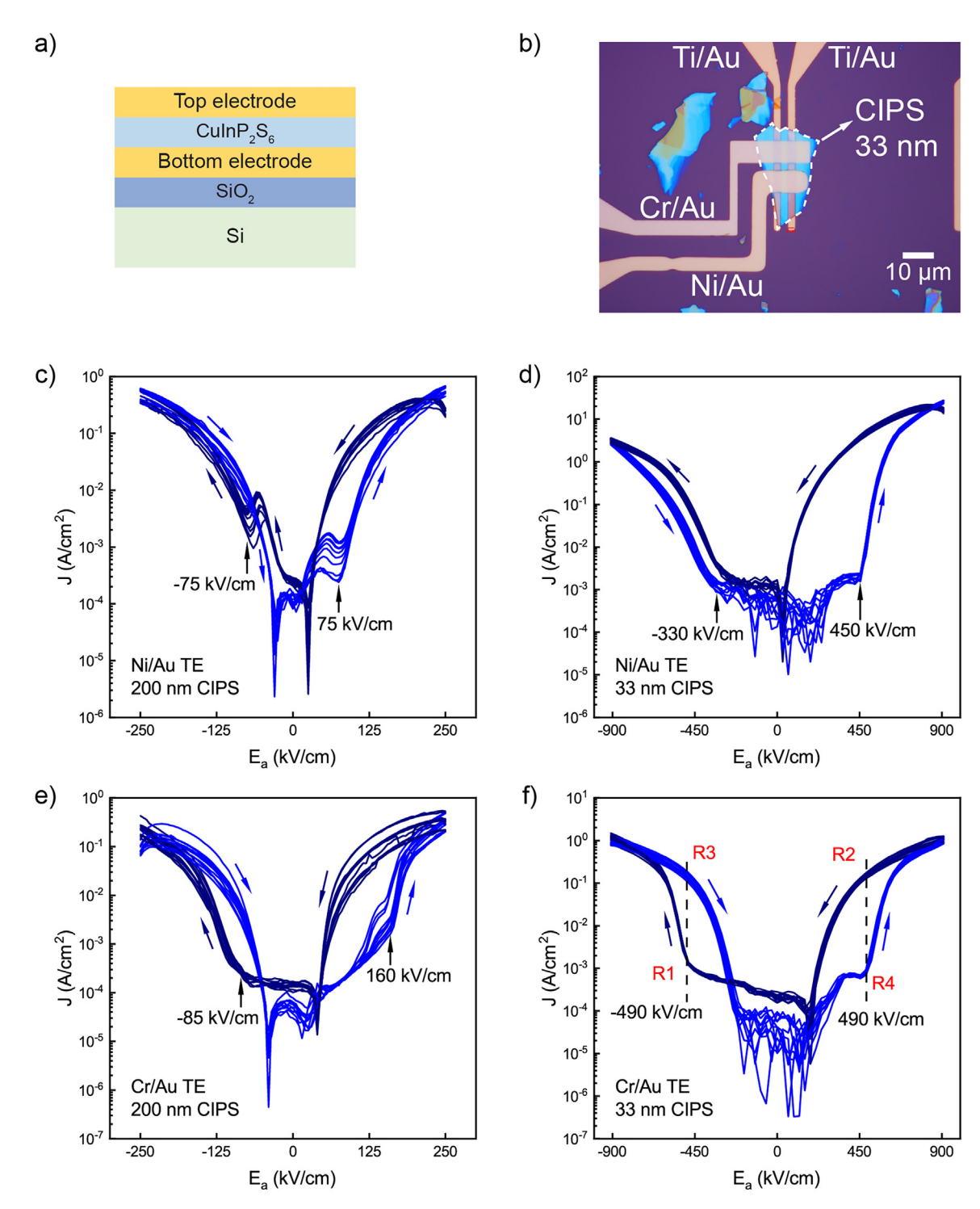


FIG. 3. Current–voltage characteristics and resistive states. (a) Schematic of our device structure. (b) Optical microscope images of two trilayer devices prepared on a 33 nm-thick crystal of CIPS with a top electrode of Cr and Ni, respectively, both of which were topped by a 30 nm thick Au layer. Other two trilayer devices were also prepared similarly on a 200 nm-thick crystal of CIPS [Fig. S1(a)]. (c)–(f) Current–voltage characteristics measured from four trilayer devices possessing either a Ni/Au or Cr/Au top TE but different thicknesses of CIPS crystals (200 and 30 nm, respectively) as indicated. Eleven hysteresis loops were recorded. Negative voltages for negative currents were converted to be positive to facilitate semi-log plotting. Positive-to-negative and negative-to-positive branches are labeled by different colors. The voltages near which a jump in current density occurs are indicated. Four resistance states [corresponding to Figs. 4(c)–4(f)] are labeled in (f).

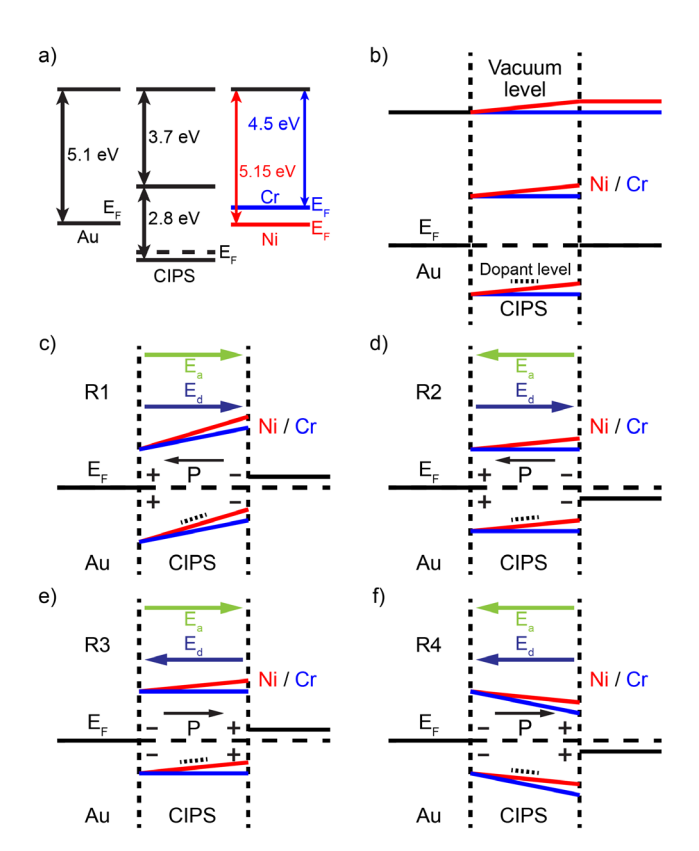


FIG. 4. Band diagrams for Au/CIPS/Cr and Au/CIPS/Ni structures. Band diagrams corresponding to (a) down pointing polarization and negative bias, (b) down pointing polarization and positive bias, (c) up pointing polarization and negative bias, and (d) up pointing polarization and positive bias.

Larger work function of Ni leads to a larger barrier height on Ni-CIPS interface. When polarization points are up, different from the Cr-33 nm device, the barrier height of Ni-CIPS interface is around similar to the one of Au-CIPS interface without bias voltage, making it the same for positive and negative bias voltages [Figs. 4(e) and 4(f)] in the Ni-33 nm sample, leading to the symmetric, relatively flat J–E_a curve at low bias voltage [Fig. 3(d)].

The combination of positive/negative bias and two ferroelectric polarization states would give four resistance states. For the Cr-33 nm device, resistance values of the two low (high) resistive states under two ferroelectric states are close, possibly due to the coincidence of the Schottky barrier height of Au-CIPS and Cr-CIPS contacts. Even though Au and Cr have very different work function values, Au-CIPS interface was formed by van der Waals transfer, while Cr-CIPS interface was formed during evaporation. When the Cr is replaced by other materials with very different work functions, such as Ni, this coincidence should not be present. Indeed, the Ni-33 nm device is seen to show four distinct resistive states.

Previous research showed that CIPS has two extra ferroelectric states with larger polarization (high polarization states).³⁰ In principle, the peaks occurred in Fig. 3(e) can correspond to the switching from low polarization to high polarization state. However, the potential barrier between high and low polarization is quite small,¹⁰ making high polarization states metastable. It is difficult to observe the transition to

high polarization states by transport measurements. Moreover, Cr-200 nm sample did not show peaks in its J–E_a curve, suggesting that observed peaks are not associated with high polarization states.

For devices of thick CIPS, the J– E_a curves show butterfly-shape hysteresis loops. For the Ni-200 nm device, two secondary peaks in the magnitude of J are seen when the magnitude of E_a was swept from low to high values in both directions. As seen in Figs. S4(e) and S4(g), the band bending leads to a "potential well" for mobile electrons migrated from TE near the CIPS/TE interface. Because of the work function difference, the "potential well" near the CIPS/TE interface for the TE of Ni is more shallow than that for Cr, which means that these electrons can be removed from the "potential well," leading to a peak in J. However, after these electrons trapped in the "potential" well are all removed, J will start to drop, leading to a negative conductance as the magnitude of E_a increases further.

With respect to the resistance ratio, for devices with Cr as the TE, the resistance ratios under positive and negative biases are similar. In the Cr-200 nm and Cr-33 nm devices, a resistance ratio $\sim\!100$ is reached. For devices with Ni as top electrodes, the resistance ratio under negative bias is much smaller than the ratio under positive bias. Resistance ratios under positive and negative bias are $\sim\!100$ and 10, respectively, for Ni-200 nm devices. The largest resistance ratio $\sim\!1800$ was obtained in the Ni-33 nm device under positive bias [under applied field $\sim\!450\,\mathrm{kV/cm}$, labeled in Fig. 3(f)]. Same as the Ni-200 nm device, resistance ratio under negative bias is much smaller, only $\sim\!6$ [under applied field $\sim\!-450\,\mathrm{kV/cm}$, labeled in Fig. 3(d)]. Four resistance states ranging from $\mathrm{M}\Omega$ to $\mathrm{G}\Omega$ were achieved in Ni-33 nm.

In conclusion, we have prepared Au/CIPS/Cr and Au/CIPS/Ni heterostructures using nanosheets of CIPS obtained by mechanical exfoliation. We found four resistive states that are determined by bias and polarization as well as switching behavior in the J– E_a characteristics, which we attribute to the formation of FSD. We also found that thicknesses of the ferroelectric semiconductor and the work functions of the electrodes play an important role for these devices. The performance of these FSDs may be optimized, making them potentially useful for nonvolatile memory applications.

See the supplementary material for optical images of Cr- and Ni-200 nm devices, extra I–V characteristics, and band diagrams for devices with thick films.

The growth of single crystals of CIPS used in this work was supported by the National Science Foundation through the Penn State 2D Crystal Consortium-Materials Innovation Platform (2DCC-MIP) under NSF cooperative Agreement Nos. DMR-1539916 and DMR-2039351. Bulk of the work, including device, characterization, and data analysis, was supported as part of the center for 3D Ferroelectric Microelectronics (3DFeM), an Energy Frontier Research Center funded by the U.S. Department of Energy (DOE), Office of Science, Basic Energy Sciences under Award Number DE-SC0021118. Useful discussions with Professor S. Trolier-Mckinstry and Professor T. Jackson are gratefully acknowledged.

AUTHOR DECLARATIONS Conflict of Interest

The authors have no conflicts to disclose.

Author Contributions

Jinyuan Yao: Conceptualization (equal); Data curation (equal); Formal analysis (equal); Writing – original draft (equal); Writing – review & editing (equal). Yongtao Liu: Data curation (supporting); Validation (supporting). Shaoqing Ding: Data curation (supporting); Validation (supporting). Yanglin Zhu: Resources (supporting). Zhiqiang Mao: Funding acquisition (supporting); Resources (supporting); Validation (supporting). Sergei V. Kalinin: Resources (supporting). Ying Liu: Conceptualization (equal); Funding acquisition (equal); Resources (equal); Validation (equal); Writing – review & editing (equal).

DATA AVAILABILITY

The data that support the findings of this study are available from the corresponding author upon reasonable request.

REFERENCES

- ¹M. Si, A. K. Saha, S. Gao, G. Qiua, J. Qin, Y. Duan, J. Jian, C. Ni, H. Wang, W. Wu, S. K. Gupta, and P. D. Ye, "A ferroelectric semiconductor field-effect transistor," Nat. Electron. **2**, 580–586 (2019).
- ²C. Wang, Z. Tang Xu, L. Wang, C. Ge, H. Bin Lu, H. Zhong Guo, M. He, G. Zhen Yang, and K. Juan Jin, "Switchable diode effect and ferroelectric resistive switching in epitaxial BiFeO₃ thin films," Appl. Phys. Lett. **98**, 192901 (2011).
- ³P. W. M. Blom, R. M. Wolf, J. F. M. Cillessen, and M. P. C. M. Krijn, "Ferroelectric Schottky diode," Phys. Rev. Lett. **73**, 2107 (1994).
- ⁴H. Matsuo, Y. Kitanaka, R. Inoue, Y. Noguchi, and M. Miyayama, "Switchable diode-effect mechanism in ferroelectric BiFeO₃ thin film capacitors," J. Appl. Phys. **118**, 114101 (2015).
- ⁵L. Pintilie, V. Stancu, L. Trupina, and I. Pintilie, "Ferroelectric Schottky diode behavior from a SrRuO₃-Pb(Zr_{0.2}Ti_{0.8})O₃-Ta structure," Phys. Rev. B **82**, 085319 (2010).
- ⁶P. van der Sluis, "Non-volatile memory cells based on Zn_xCd_{1-x}S ferroelectric Schottky diodes," Appl. Phys. Lett. **82**, 4089 (2003).
- ⁷T. Eshita, T. Tamura, and Y. Arimoto, 14 Ferroelectric Random Access Memory (FRAM) Devices, Advances in Non-Volatile Memory and Storage Technology (Woodhead Publishing, 2014).
- ⁸V. Maisonneuve, V. B. Cajipe, A. Simon, R. V. D. Muhll, and J. Ravez, "Ferrielectric ordering in lamellar CuInP₂S₆," Phys. Rev. B **56**, 10860 (1997).
- ⁹A. Simon, J. Ravez, V. Maisonneuve, C. Payen, and V. B. Cajipe, "Paraelectric-ferroelectric transition in the lamellar thiophosphate CuInP₂S₆," Chem. Mater. 6, 1575 (1994).
- ¹⁰S. Zhou, L. You, A. Chaturvedi, S. A. Morris, J. S. Herrin, N. Zhang, A. Abdelsamie, Y. Hu, J. Chen, Y. Zhou, S. Dong, and J. Wang, "Anomalous polarization switching and permanent retention in a ferroelectric ionic conductor," Mater. Horiz. 7, 263 (2020).
- ¹¹F. Liu, L. You, K. L. Seyler, X. Li, P. Yu, J. Lin, X. Wang, J. Zhou, H. Wang, H. He, S. T. Pantelides, W. Zhou, P. Sharma, X. Xu, P. M. Ajayan, J. Wang, and Z. Liu, "Room-temperature ferroelectricity in CuInP₂S₆ ultrathin flakes," Nat. Commun. 7, 12357 (2016).
- $^{12}\text{W}.$ F. Io, M.-C. Wong, S.-Y. Pang, Y. Zhao, R. Ding, F. Guo, and J. Hao, "Strong piezoelectric response in layered CuInP₂S₆ nanosheets for piezoelectric nanogenerators," Nano Energy **99**, 107371 (2022).

- ¹³V. Samulionis, J. Banys, Y. Vysochanskii, and V. Cajipe, "Elastic and electromechanical properties of new ferroelectric-semiconductor materials of Sn₂P₂S₆ family," Ferroelectrics 257, 113 (2001).
- ¹⁴P. Yu, F. Wang, J. Meng, T. A. Shifa, M. G. Sendeku, J. Fang, S. Li, Z. Cheng, X. Lou, and J. He, "Few-layered CuInP₂S₆ nanosheet with sulfur vacancy boosting photocatalytic hydrogen evolution," CrystEngComm 23, 591 (2021).
- photocatalytic hydrogen evolution," CrystEngComm 23, 591 (2021).

 15 S. Zhou, L. You, H. Zhou, Y. Pu, Z. Gui, and J. Wang, "Van der Waals layered ferroelectric CuInP₂S₆: Physical properties and device applications," Front. Phys. 16, 13301 (2021).
- 16B. Li, S. Li, H. Wang, L. Chen, L. Liu, X. Feng, Y. Li, J. Chen, X. Gong, and K.-W. Ang, "An electronic synapse based on 2d ferroelectric CuInP₂S₆," Adv. Electron. Mater. 6, 2000760 (2020).
- ¹⁷M. Si, P.-Y. Liao, G. Qiu, Y. Duan, and P. D. Ye, "Ferroelectric field-effect transistors based on MoS₂ and CuInP₂S₆ two-dimensional van der Waals heterostructure," ACS Nano 12, 6700 (2018).
- ¹⁸X. Jiang, X. Wang, X. Z. X. Wang, R. Niu, J. Deng, S. Xu, Y. Lun, Y. Liu, T. Xia, J. Lu, and J. Hong, "Manipulation of current rectification in van der Waals ferroionic CuInP₂S₆," Nat. Commun. 13, 574 (2022).
- ¹⁹F. Kong, L. Zhang, T. Cong, Z. Wu, K. Liu, C. Sun, L. Pan, and D. Li, "Tunable photochemical deposition of silver nanostructures on layered ferroelectric CuInP₂S₆," J. Appl. Phys. 132, 044103 (2022).
- ²⁰ J. Chen, C. Zhu, G. Cao, H. Liu, R. Bian, J. Wang, C. Li, J. Chen, Q. Fu, Q. Liu, P. Meng, W. Li, F. Liu, and Z. Liu, "Mimicking neuroplasticity via ion migration in van der Waals layered copper indium thiophosphate," Adv. Mater. 34, 2104676 (2022).
- ²¹Y. Ding, X. Xu, A. Bhalla, X. Yang, J. Chen, and C. Chen, "Switchable diode effect in BaZrO₃ thin films," RSC Adv. 6, 60074 (2016).
- ²²Y. Guo, B. Guo, W. Dong, H. Li, and H. Liu, "Evidence for oxygen vacancy or ferroelectric polarization induced switchable diode and photovoltaic effects in BiFeO₃ based thin films," Nanotechnology 24, 275201 (2013).
- ²³L. Niu, F. Liu, Q. Zeng, X. Zhu, Y. Wang, P. Yu, J. Shi, J. Lin, J. Zhou, Q. Fu, W. Zhou, T. Yu, X. Liu, and Z. Liu, "Controlled synthesis and room-temperature pyroelectricity of CuInP₂S_c ultrathin flakes," Nano Energy 58, 596 (2019).
- pyroelectricity of CuInP_2S_6 ultrathin flakes," Nano Energy **58**, 596 (2019).
 ²⁴Z. Zhao, K. Xu, H. Ryu, and W. Zhu, "Strong temperature effect on the ferroelectric properties of CuInP_2S_6 and its heterostructures," ACS Appl. Mater. Interfaces **12**, 51820 (2020).
- ²⁵S. N. Neal, S. Singh, X. Fang, C. Won, F. t Huang, S.-W. Cheong, K. M. Rabe, D. Vanderbilt, and J. L. Musfeldt, "Vibrational properties of CuInP₂S₆ across the ferroelectric transition," Phys. Rev. B 105, 075151 (2022).
- ²⁶J. H. Lee, J. H. Jeon, C. Yoon, S. Lee, Y. S. Kim, T. J. Oh, Y. H. Kim, J. Park, T. K. Song, and B. H. Park, "Intrinsic defect-mediated conduction and resistive switching in multiferroic BiFeO₃ thin films epitaxially grown on SrRuO₃ bottom electrodes," Appl. Phys. Lett. 108, 112902 (2016).
- 27D. Zhang, Z.-D. Luo, Y. Yao, P. Schoenherr, C. Sha, Y. Pan, P. Sharma, M. Alexe, and J. Seidel, "Anisotropic ion migration and electronic conduction in van der Waals ferroelectric CuInP₂S₆," Nano Lett. 21, 995 (2021).
- ²⁸S. M. Neumayer, M. Si, J. Li, P.-Y. Liao, L. Tao, A. O'Hara, S. T. Pantelides, P. D. Ye, P. Maksymovych, and N. Balke, "Ionic control over ferroelectricity in 2D layered van der Waals capacitors," ACS Appl. Mater. Interfaces 14, 3018 (2022).
- ²⁹D. A. Neamen, Semiconductor Physics and Devices: Basic Principles, 4th ed. (The McGraw-Hill Companies, Inc., New York, 2012).
- 30). A. Brehm, S. M. Neumayer, L. Tao, A. O'Hara, M. Chyasnavichus, M. A. Susner, M. A. McGuire, S. V. Kalinin, S. Jesse, P. Ganesh, S. T. Pantelides, P. Maksymovych, and N. Balke, "Tunable quadruple-well ferroelectric van der Waals crystals," Nat. Mater. 19, 43 (2020).